Biosensors and Bioelectronics 35 (2012) 284–290

Contents lists available at SciVerse ScienceDirect

Biosensors and Bioelectronics

journal homepage: www.elsevier.com/locate/bios

# A quantitative study of detection mechanism of a label-free impedance biosensor using ultrananocrystalline diamond microelectrode array

Shabnam Siddiqui[a], Zhenting Dai[a], Courtney J. Stavis[b], Hongjun Zeng[a], Nicolaie Moldovan[a], Robert J. Hamers[b], John A. Carlisle[a], Prabhu U. Arumugam[a,*]

[a] Advanced Diamond Technologies, Inc., 429 B Weber Road #286, Romeoville, IL 60446, USA
[b] Department of Chemistry, University of Wisconsin, 1101 University Avenue, Madison, WI 53706, USA

ARTICLE INFO

*Article history:*
Received 8 December 2011
Received in revised form 16 February 2012
Accepted 2 March 2012
Available online 10 March 2012

*Keywords:*
Nanocrystalline diamond
Electrochemical impedance spectroscopy
Microelectrode array
Water-borne pathogen
Label-free
Biosensor

ABSTRACT

It is well recognized that label-free biosensors are the only class of sensors that can rapidly detect antigens in real-time and provide remote environmental monitoring and point-of-care diagnosis that is low-cost, specific, and sensitive. Electrical impedance spectroscopy (EIS) based label-free biosensors have been used to detect a wide variety of antigens including bacteria, viruses, DNA, and proteins due to the simplicity of their detection technique. However, their commercial development has been hindered due to difficulty in interpreting the change in impedance upon antigen binding and poor signal reproducibility as a result of surface fouling and non-specific binding. In this study, we develop a circuit model to adequately describe the physical changes at bio functionalized surface and provide an understanding of the detection mechanism based on electron exchange between electrolyte and surface through pores surrounding antibody–antigen. The model was successfully applied to extract quantitative information about the bio surface at different stages of surface functionalization. Further, we demonstrate boron-doped ultrananocrystalline diamond (UNCD) microelectrode array (3 × 3 format, 200 μm diameter) improves signal reproducibility significantly and increases sensitivity by four orders of magnitude. This study marks the first demonstration of UNCD array based biosensor that can reliably detect a model *Escherichia coli K12* bacterium using EIS, positioning this technology for rapid adoption in point-of-use applications.



## 1. Introduction

Electrochemical impedance spectroscopy (EIS) is widely used to investigate the electrochemical properties of materials, electrode processes and interfaces (Long et al., 2003; Ma et al., 2006; Szpak, 1991). EIS based label-free biosensors (Zheng et al., 2005; Cui et al., 2001; Stern et al., 2010; Nirschl et al., 2011) are the most promising for detection of antigens (Katz and Willner, 2003; Daniels and Pourmand, 2007; Ghindilis, 2009) due to simplicity in transducing the detection signal and high sensitivity in monitoring the changes occurring at the interface. In EIS technique, a sinusoidal signal $v(t) = V_m \sin(\omega t)$, is applied to the electrode and the resulting current $i(t) = I_m \sin(\omega t + \theta)$ is measured ($V_m$ is voltage amplitude, $\omega$ is frequency, $I_m$ is current amplitude, $\theta$ is phase). The ratio $v(t)/i(t)$ at a particular frequency is defined as the impedance ($Z$) of the cell. This measurement is repeated at different frequencies, yielding $Z(\omega)$. The electrode–cell system behavior is then investigated by fitting experimental impedance data to an equivalent circuit model. In EIS biosensors, the change in impedance after antigen binding to the bio-functionalized electrode surface that is modified with monolayers and receptors (oligonucleotide, DNA, antibody, aptamer) is typically interpreted as detection. This change in impedance is analyzed by fitting the data to Randles circuit that consists of an uncompensated resistance ($R_S$) in series with the parallel combination of the capacitance ($C$) and a charge transfer resistance ($R_{ct}$) of a faradic reaction (Long et al., 2003; Yu et al., 2006). The change in $R_{ct}$ upon antigen binding is proportional to antigen concentration and thus provides quantitative information. However, the Randles circuit is too simplistic to model real electrochemical systems such as biosensors and does not adequately describe the physical changes at the electrode interface. Interpreting change in impedance as detection without proper understanding of what causes such a change can lead to a misleading interpretation of experimental data. Here, we address this first problem by presenting a possible explanation for the change in impedance by constructing a new circuit model that fits well to experimental data. Each circuit element provides a quantitative measure of the physical changes at the electrode surface as a function of antigen binding to antibodies. Secondly, selectivity, another important feature for a biosensor, is usually demonstrated using positive and negative control experiments

* Corresponding author.
*E-mail address:* prabhu@thindiamond.com (P.U. Arumugam).

0956-5663/$ – see front matter © 2012 Elsevier B.V. All rights reserved.
doi:10.1016/j.bios.2012.03.001

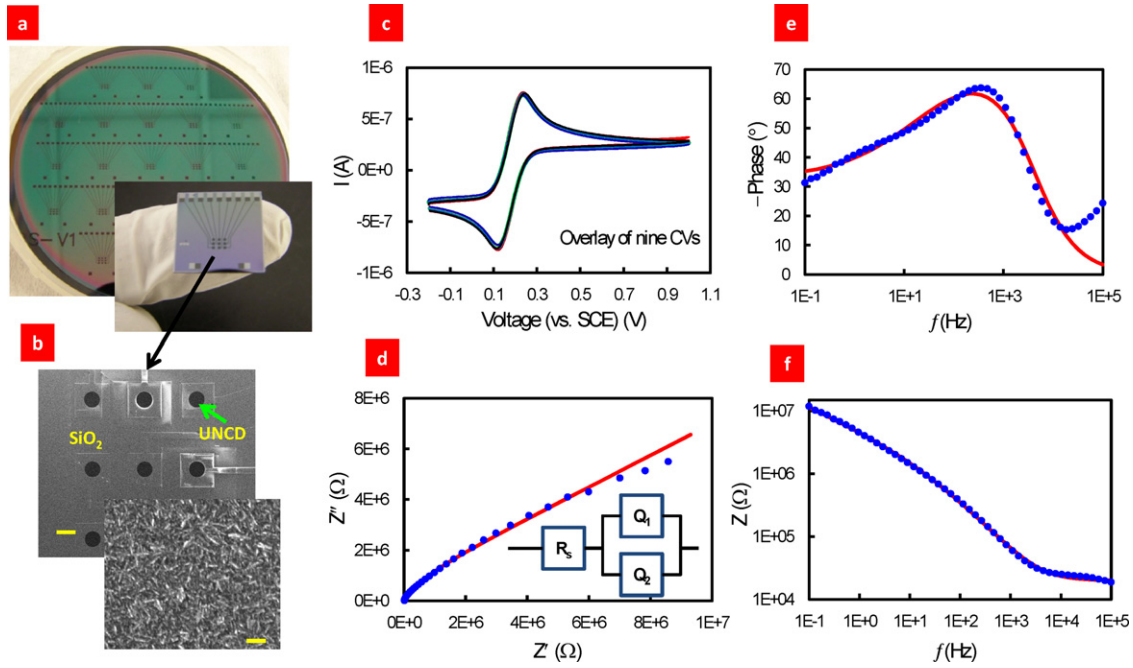


**Fig. 1.** (a) Optical image of UNCD planar 3 × 3 microelectrode array (MEA) fabricated in a 4 in. silicon wafer. (b) SEM image of one of the chips showing the nine individually addressable microelectrodes and the inset showing the UNCD surface morphology. (c) Cyclic voltammograms of all nine microelectrodes in a chip. Scan rate is 100 mV/s. (d–f) EIS characterization of un-modified "bare" UNCD microelectrodes: Nyquist and Bode plots. The data is fitted to [$R_s$ ($Q_1$ $Q_2$)] circuit model (inset, d) (dotted curve-experimental and solid curve-fitted). The electrolyte is 5 mM $Fe(CN)_6^{3-/4-}$ in 0.01 M PBS buffer. The scale bar in (b) is 200 and 0.2 μm (inset).

(Ma et al., 2006). For these experiments, surfaces are functionalized with matched and mismatched antibodies. The difference between the two $R_{ct}$ values obtained from these two surfaces provides a quantitative measure of antigen present in the sample. A major limitation of this approach is that at very low antigen concentrations, the difference between the signals from matched antibody (*i.e.* the positive signal) and mismatched antibody (*i.e.* the false-positive signal due to non-specific binding) become very small or negligible, and thus prevents detection of very low concentrations of antigen. A critical feature of the proposed model is that it can differentiate between a positive signal and a false-positive signal without performing any control experiments. Thirdly, to achieve higher signal reproducibility and sensitivity, we have used an ultrananocrystalline diamond (UNCD) microelectrode array (MEA) (Fig. 1a and b) (details in methods section). It is well established that diamond (Yang et al., 2002; Sun et al., 2007; Nebel et al., 2007) is an extremely chemically stable electrode material with a wide electrochemical potential window, low background currents, reduced non-specific protein binding, dimensional stability, and the ability to regenerate the surface multiple cycles (Alehashem et al., 1995; Show et al., 2003; Clare et al., 2005; Stavis et al., 2011). Recently, Radadia (Radadia et al., 2011) demonstrated that anti-*Escherichia coli* O157:H7 functionalized ultra-smooth (5–8 nm rms) UNCD substrates (Gruen et al., 1996) are much more stable, selective and resist non-specific binding as compared to Corning® glass substrates (GAPSII). Smaller electrode sizes are well-known to increase faradic current due to enhanced mass-transport and reduce the non-faradic "charging" currents. Hence, increases the signal-to-noise ratio, *i.e.* higher sensitivity (Yang et al., 2011). All these characteristics allow UNCD MEA to be an ideal interface for biosensing.

In this study, boron-doped conductive UNCD films were grown on 4-inch silicon wafers using a hot filament chemical vapor deposition (HFCVD) technique (Moldovan et al., 2009). Three types of UNCD electrodes were examined: (1) an un-patterned continuous film (4 mm diameter, defined by O-ring size in electrochemical cell), (2) a shorted array where all nine microelectrodes (200 μm in diameter) in the array are electrically connected, and (3) a patterned array where the microelectrodes are individually electrically addressable. For the first time, we report a 3 × 3-UNCD array EIS biosensor for *E. coli K12* detection. High S/N ratio and on-chip multiple analyte detection with built-in control experiments could be achieved with such arrays. We also confirm the feasibility of a reliable wafer-scale fabrication process that utilizes standard semiconductor processes and can be scaled up to $N \times N$ arrays (with $N$ up to 10), critical for the development of highly multiplexing biosensor chips.

## 2. Materials and methods

### 2.1. UNCD microarray fabrication

Four inch silicon wafers with a surface coating of 1 μm-thick thermal $SiO_2$ (Wafer World) were used to grow a 2 μm-thick UNCD film. The electrical conductivity of the film was <0.1 Ω cm based on 4-probe measurements (Pro4, Lucas Labs, Gilroy, CA). The average roughness of the UNCD film was <10 nm rms based on AFM measurements (Digital Instruments, Santa Barbara, CA). Optical microlithography was used to fabricate 21 chips per wafer. Each chip was micro patterned into nine individually addressable 200 μm diameter disk microelectrodes in a 3 × 3 array format (Fig. 1a and b). Briefly, the micro fabrication steps were as follows: (a) deposit a 500 nm thick $SiO_2$ layer using Plasma Enhanced CVD (PECVD); (b) pattern oxide using a 1.7 μm thick positive resist; (c) wet etch the oxide in 10:1 Buffered Oxide Etchant for 15 min; (d) dry etch the UNCD with reactive ion etching (ICP-RIE) of $O_2/SF_6$ gas mixture (Moldovan et al., 2009) through the oxide hard mask formed in the previous steps to form MEAs, electrical contact pads and the electrical lines between them; (e) deposit another 500 nm thick $SiO_2$ PECVD film; and (f) wet etch $SiO_2$ to open up the UNCD microelectrode (200 μm diameter) array and the contact pads. The final $SiO_2$ film was 1 μm thick and found to be adequate to passivate the underlying UNCD form the electrolyte solution.

Surface characterization using SEM and optical microscopy showed no major defects and/or contamination of the electrode surface. The UNCD electrode surface is more oxidized and hydrophilic than the as-deposited surface. This is because the surface is exposed with strongly oxidizing chemicals during micro fabrication and acquires hydrophilic groups. To achieve higher efficiencies during photochemical grafting of biomolecules, the surface is preferentially hydrogen terminated by exposing the UNCD surface to an atomic hydrogen environment in HFCVD chamber for 15 min at 8 Torr.

### 2.2. UNCD bio functionalization

All stock solutions were prepared using deionized water from a Millipore water purification system to obtain a minimum resistivity of 18.0 MΩ cm. Casein blocking solution, 1-dodecene, sodium borohydride, phosphate-buffered saline (PBS) and PBS with Tween 20 were obtained from Sigma–Aldrich. Methanol and ethanol was obtained from Fisher Scientific. Nitrogen (Air gas Inc.) was used after filtering it through a 0.22 μm Teflon filter. UNCD MEAs were functionalized with anti-*E. coli K12* as described previously (Stavis et al., 2011; Radadia et al., 2011) with the following modifications. Functionalized surfaces were incubated overnight (20 h, 4 °C) with an anti-*E. coli K12* antibody solution (50 μg/ml) in a home-made polycarbonate well. The wells were sealed with a sterile aluminum adhesive film. On the next day, the chips were washed to remove non-specifically bound antibodies. The washing routine used in the experiments consisted of rinsing with PBS-Tween20 twice followed by PBS once. Non-specific binding sites on surfaces were blocked using casein blocking solution (45 min, 32 °C). For control experiments, all the above steps were carried out except the antibody attachment step. For *E. coli K12* capture assay, heat-kill ed *E. coli K12* culture (80 °C for 15 min) was used for bacteria capture experiments. The heat-killed culture was agar plated for 48 h and showed no bacterial viability. The stock was diluted to a final concentration of ~$1.0 \times 10^7$ cfu/ml and deposited on antibody-functionalized surfaces. Bacteria capture was performed at 37 °C for 60 min with constant shaking. Evaporation from wells was minimized using adhesive aluminum film. At the end of the capture step, to remove the excess bacterial solution, surfaces were washed with PBS (thrice) to remove non-specifically bound bacteria.

### 2.3. Electrochemical measurements

All EC experiments were carried out with an Autolab potentiostat (PGSTAT 302N, Metrohm USA) in a three-electrode setup using a Pt coil (Alfa Aesar) counter electrode and a saturated calomel electrode (SCE, Accumet, New Hampshire, USA) as the reference electrode. The potentiostat was equipped with Frequency Response Analyzer 2, ECD and Multiplex modules and Nova 1.7 software. The UNCD MEA was used as the working electrode. The electrode surfaces were exposed to the solution and sealed with a 4 mm diameter O-ring in a Teflon cell. For each sensor array chip, the electrical isolation of the pads was checked using a two-point probe multimeter. This ensures the integrity of the $SiO_2$ passivation, which is essential for stable sensors. Prior to characterization, MEA were briefly sonicated in ethanol for 30 s and dried in $N_2$. Cyclic voltammograms (CV) were recorded between −0.2 and +1.0 V *vs.* SCE with a scan rate of 100 mV/s. The EIS spectra were recorded between 100 kHz and 100 mHz at 10 mV ac signal amplitude (rms value) at a 0 DC voltage. All measurements were carried out in a solution of 5 mM $K_4Fe(CN)_6$/5 mM $K_3Fe(CN)_6$ in 0.01 M phosphate buffer (pH 7.4).

## 3. Results and discussion

### 3.1. Electrochemical characterization of un-modified UNCD surface

The cyclic voltammogram (CV) in 5 mM $K_4Fe(CN)_6$/5 mM $K_3Fe(CN)_6$ in 0.01 M phosphate buffer (pH 7.4) (Fig. 1c) showed a quasi-reversible behavior with a separation in reduction-oxidation "redox" peak potential ($\Delta E_p$) of ~110 mV, similar to ones found in the literature (Granger et al., 2000; Li et al., 2005). A high yield (>80% microelectrodes in the array working) and a <5% variation in CV peak current, $I_p$ ($I_p$ being directly proportional to electrode area) and $\Delta E_p$ among the microelectrodes in an array demonstrates the reliability of the micro fabrication process. EIS measurements were performed at three stages in the biosensor fabrication (Fig. S1, in Supporting information): (i) on the un-modified "bare" surface (step 0), (ii) after anti-*E. coli K12* attachment and casein blocker deposition (step 5) and (iii) after *E. coli K12* bacteria capture (step 6). Casein was used as a blocker instead of bovine serum albumin or protein-free block because it reduces non-specific binding on UNCD surfaces (Radadia et al., 2011). A 0 V DC was applied because in impedance biosensors, the DC bias voltages should be quite small to avoid disturbing the probe layer. Also, monolayers are covalently attached to the electrode with a binding energy of the order of few electron volts; applying a relatively high voltage of 200 mV would break these bonds. The covalent bond energies are on the order of few electron volts but probe-target binding energies can be much less. Thus, applying a relatively high voltage of 200 mV would break these bonds and/or destabilize the interface by applying a force on charged molecules (Daniels and Pourmand, 2007; Schulz et al., 2007). The bare electrode experimental data fits well to an equivalent circuit model [$R_s$ ($Q_1Q_2$)] that has two constant phase elements ($Q_1$,$Q_2$). Table 1 show values of circuit elements ($R_s$, $Q_1$, $N_1$, $Q_2$ and $N_2$) for the microelectrodes in the array. The presence of constant phase element (CPE) is indicative of time-constant or capacitive dispersion. CPE behavior could arise from surface heterogeneities such as grain boundaries, crystal faces on a polycrystalline diamond, or other variations in surface properties for *e.g.* surface conductivity or surface roughness. Even though several groups have characterized diamond films using impedance spectroscopy (Ramesham and Rose, 1997; Juttner and Becker, 2007), the actual causes for CPE behavior of diamond is not well understood. The impedance due to CPE is commonly represented as $Z(\omega) = (1/Q(j\omega)^N)$ (Barsoukov and MacDonald, 2005). Here, the parameters $N$ and $Q$ are independent of frequency. For $N = 1$, $Q$ represents pure capacitance, for $N = 0$, $Q$ behaves as resistor, for $N = -1$, $Q$ behaves as inductor and for $0 < N < 1$, represent CPE behavior. Since UNCD is composed of phase pure $sp^3$-bonded grains (~2–5 nm) separated by atomically abrupt $sp^2$ grain boundaries (Gruen et al., 1996), the two values of $Q$ are presumably due to them. It is well-known that the crystalline diamond surface is

**Table 1**
Values of interfacial parameters of un-modified UNCD microelectrodes obtained by fitting [$R_s$ ($Q_1Q_2$)] circuit to experimental data. The % error in the values of parameters $R_s$, $Q_1$, $N_1$, $Q_2$, $N_2$ are 0–2%, 4–7%, 2–5%, 15–20%, and 2–5%.

| Microelectrode # | $R_s$ (KΩ) | $Q_1$ (nMho $s^n$) | $N_1$ | $Q_2$ (nMho $s^n$) | $N_2$ |
|---|---|---|---|---|---|
| 1 | 20.1 | 7.86 | 0.868 | 99.7 | 0.367 |
| 2 | 17.0 | 8.52 | 0.871 | 134 | 0.317 |
| 3 | 13.8 | 5.74 | 0.899 | 110 | 0.349 |
| 4 | 14.6 | 7.28 | 0.878 | 102 | 0.355 |
| 5 | 13.8 | 4.46 | 0.925 | 99.4 | 0.416 |
| 6 | 15.8 | 7.34 | 0.875 | 114 | 0.338 |
| 7 | 14.4 | 3.64 | 0.936 | 116 | 0.362 |
| 8 | 16.4 | 6.09 | 0.889 | 103 | 0.366 |
| 9 | 18.4 | 7.89 | 0.858 | 110 | 0.344 |

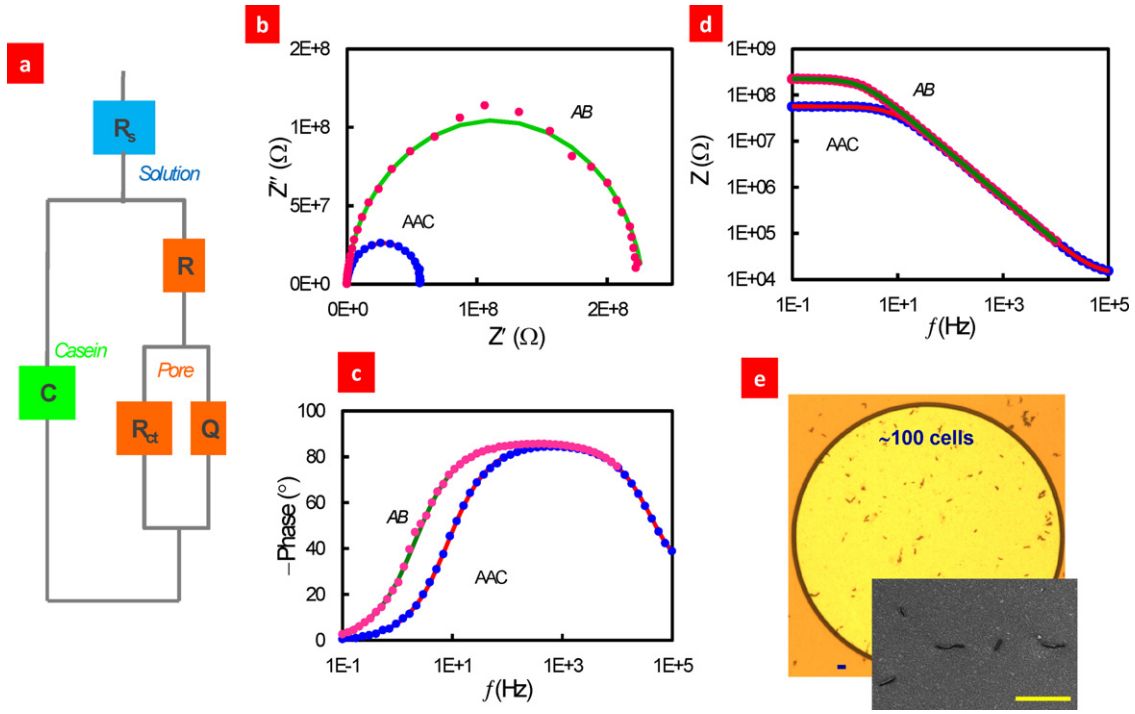


**Fig. 2.** (a) The equivalent circuit model fitted to experimental data of UNCD surface modified with antibody and bacteria capture. The origin of the various circuit parameters is shown in different color squares: blue – uncompensated solution resistance; green – from casein layer and orange – from pores. (b–d) Nyquist, Bode phase and Bode modulus plots (dotted curve-experimental and solid curve-fitted) obtained after antibodies and casein blocker (AAC) and after bacteria capture (AB). (e) The optical and SEM (inset) images of *E. coli K12* captured on microelectrode. The electrolyte used is 5 mM $Fe(CN)_6^{3-/4-}$ in 0.01 M PBS buffer. The antibody and bacteria concentration is ~50 μg/ml and $\sim 1.0 \times 10^7$ cfu/ml, respectively. The scale bar in (e) is 3 μm and 8 μm (inset). (For interpretation of the references to color in this figure legend, the reader is referred to the web version of the article.)

more homogenous in surface morphology than grain boundaries (Hernando et al., 2009; Kondo et al., 2003); therefore higher $N$ values (homogenous surface morphology) can be attributed to grains (*i.e.* $N_1$ in Table 1), and lower $N$ values to grain boundaries ($N_2$). From Table 1, the value of $Q$ corresponding to grains ($Q_1$) is lower than that of grain boundaries ($Q_2$). While higher $Q$ corresponds to low impedance, grain boundaries are more conductive than grains. This agrees with the observation reported by Swain et al. (Holt et al., 2004) as they showed that concentration of boron dopants is higher in grain boundaries than in grains causing higher conductivity. This observation of unique "two-$Q$ behavior" of UNCD surface shows that time-constant dispersion arising due to grains can be distinguished from that of grain boundaries. This $[R_s\,(Q_1Q_2)]$ model could be generally helpful in understanding the structural and electrical conductivity changes occurring at grain-grain boundary level in polycrystalline diamond films under different electrochemical environments, *e.g.* advanced oxidation of organics.

### 3.2. Electrochemical "pore" model for antibody-modified UNCD surface

The Nyquist and Bode plots after anti-*E. coli K12* antibody attachment and deposition of a casein blocker (step 5) are shown in Fig. 2b–d. The impedance response changed from a linear spectrum to a semi-circle, *i.e.* the faradic process is kinetically controlled without any significant mass-transfer (diffusion) effects. Since the electrode surface has been modified, a different equivalent circuit model (Fig. 2a) was fitted to the experimental data and the value of the different parameters thus obtained is shown in Table 2. The interpretation of the circuit parameters are as follows: $R_s$ is uncompensated resistance; $C$ is a capacitance that arises due to coverage of the electrode surface with casein; $R_{ct}$ is a charge transfer resistance that arises due to resistance to the exchange of electrons between electrode and $Fe(CN)_6^{3-/4-}$ redox couple in the pores where antibodies are immobilized (Fig. S2a, in Supporting information), $R$ is electrolyte resistance in the pore and $Q$ is the CPE arising due to UNCD grains exposed in the pores because the value of $N$ (~0.86) corresponding to $Q$ here is same as that of $N$ of grains of bare electrode. The pores are formed only in those places where antibodies are immobilized and all remaining surface is covered with casein. The casein layer makes the electrode surface more homogenous and generates ultra-low capacitance of the order of picofarads and high impedance. Thus, casein behaves as an insulator. It is in the pores that the bare electrode surface is exposed to electrolyte and electron transfer between electrode and $Fe(CN)_6^{3-/4-}$ redox couple takes place (Fig. 2Sa, in Supporting information). It is interesting to note that the value of N in the pores has almost the same value as that of bare electrode surface, but the value of $Q$ has reduced from nanoMho $s^n$ to picoMho $s^n$ *i.e.* the electrode kinetics became very sluggish. This lowering of the $Q$ value is expected since the addition of monolayers and attachment of antibodies to these monolayers must increase impedance. If the fraction of the area covered by casein (non-electrochemically active) is $\gamma$, then the remaining fractional uncovered area is $1-\gamma$ and is the area of the pores, which is defined here as effective area that is electrochemically active. The total impedance of the cell will be the sum of impedances of the pores and that due to casein, as shown in the circuit model. The effect of electrode surface modification must manifest itself in a parameter that depends critically on electrode properties such as kinetics. In electrochemistry, one such parameter is the exchange current ($I_0$). It is defined as the current that solely depends on the exchange of electrons between electrolyte and electrode at equilibrium *i.e.* when anodic and cathodic currents are equal, *i.e.* net current is zero. For our system, the addition of monolayers to a UNCD microelectrode reduces the effective electrode area, slows electrode kinetics and increases

**Table 2**
Values of interfacial parameters of modified UNCD microelectrodes after antibody/casein and bacteria capture obtained by fitting circuit (Fig. 2a) to experimental data. The % error in the values of parameters $R_s$, $C$, $R$, $Q$, $N$ and $R_{ct}$ are 0–2%, 0–3%, 15–20%, 2–5%, 1–4% and 1–2%. For this circuit, $\chi^2 \approx 0.0015723$ and thus satisfies best fit circuit criterion.

| Microelectrode # | Step # | $R_s$ (KΩ) | $C$ (pF) | $R$ (KΩ) | $Q$ (pMho $s^n$) | $N$ | $R_{ct1}$ (MΩ) | $R_{ct2}$ (MΩ) | $R_{ct1}/R_{ct2}$ |
|---|---|---|---|---|---|---|---|---|---|
| 3 | 5 | 11.9 | 199 | 101 | 241 | 0.864 | 57 | – | 3.94 |
| | 6 | 16.9 | 244 | 2740 | 168 | 0.815 | – | 225 | |
| 4 | 5 | 12.2 | 200 | 91.5 | 217 | 0.873 | 17.7 | – | 4.14 |
| | 6 | 17.2 | 241 | 3020 | 142 | 0.836 | – | 73.4 | |
| 5 | 5 | 12.0 | 226 | 79 | 268 | 0.859 | 6.6 | – | 1.42 |
| | 6 | 15.6 | 284 | 2210 | 262 | 0.805 | – | 9.37 | |
| 8 | 5 | 14.0 | 187 | 87 | 200 | 0.885 | 13.5 | – | 3.81 |
| | 6 | 18.4 | 244 | 3270 | 139 | 0.834 | – | 51.4 | |
| 9 | 5 | 16.0 | 173 | 70 | 200 | 0.908 | 16.9 | – | 6.1 |
| | 6 | 41.1 | 205 | 827 | 208 | 0.854 | – | 103 | |

resistance to the transfer of electrons between the electrode and a $Fe(CN)_6^{3-/4-}$ redox couple. For this modified microelectrode system we found that the net current $I < 1$ nA, obtained from cyclic voltammetry curves at 0 V DC, *i.e.* $\eta \sim -180$ mV, where $\eta$ is overpotential ($\eta = E - E^0$). The very low net current values in the system suggest that the dominant current flowing is $I_0$ of modified electrode. In that circumstance, even though $\eta$ is not zero (*i.e.* non-equilibrium conditions); with net current being insignificant and assuming that there are no significant mass-transfer effects, Eq. (1) gives the expression for exchange current for our system (details shown in Supporting information).

$$I_0 = FAk^0 C\, e^{-\alpha f(E-E^0)} \tag{1}$$

where $F$ is Faraday constant, $A$ is the area of electrode, $k^0$ is the standard heterogeneous rate constant, $f$ is $F/RT = 38.92\ V^{-1}$, $\alpha$ is the transfer coefficient (0.3–0.7), $C$ is the bulk concentration, $E$ is the applied potential, $E^0$ is the formal potential of the redox couple, $n$ is the number of electrons transferred per molecule of the redox molecule, $R$ is the universal gas constant and $T$ is the temperature. From Eq. (1) we can obtain the following relationship between $R_{ct}$ and $I_0$ (details in Supporting information).

$$R_{ct} = -\left(\frac{1}{\alpha f I_0}\right) \mathrm{Log}\left(\frac{I_0}{I_0^{eq}}\right) \tag{2}$$

where $I_0^{eq}$ is the exchange current at equilibrium ($\eta = 0$). A decrease in $I_0$ causes an increase in $R_{ct}$ as shown in Eq. (2), which is validated using experimental data (Fig. S3, in Supporting information). Therefore, as the electrode kinetics slows, the effective (electro active) area of the electrode is reduced, the modified exchange current becomes small, and the charge transfer resistance increases.

Hence after step 5, we observe a transformation in the impedance behavior from a linear spectrum (Fig. 1d) to a semicircle on the Nyquist plot, as shown in Fig. 2c. In a previous study, the author reported a similar dependence of $R_{ct}$ on the effective area of the electrode (Siddiqui et al., 2010). As shown in Table 2, the value of $R_{ct}$ for all microelectrodes varies between 6.6 MΩ and 57 MΩ. It is important to note that the value of $R_{ct}$ is a suitable indicator of the density of antibody, *i.e.* higher values of $R_{ct}$ suggests an electrode surface with a high density of antibody. It can be seen that microelectrode 3 has the highest $R_{ct}$ value (57 MΩ) whereas microelectrodes 4 and 9 have similar $R_{ct}$'s (17.7 and 16.9 MΩ). Here, it is important to investigate whether this increase in $R_{ct}$ is due to antibodies only or if non-specific binding has contributed to this increase. To answer this question, it is reasonable to argue that if this increase in $R_{ct}$ is mainly due to antibodies then all of the microelectrodes after bacteria capture should show a corresponding increase in $R_{ct}$, assuming all bacteria capture is highly specific. Otherwise, a wide variation in the values of $R_{ct}$ after the bacteria capture would be observed (as discussed in next section). Preferably, the variation in $R_{ct}$ values among the modified microelectrodes should be kept at minimum for high reproducibility. The possible reasons for such variations are chemical and thermal instability of TFAAD-dodecene monolayers and their non-uniform arrangement on the electrode surface and inconsistencies in antibody density on microelectrodes within an array and from one array to another. This could be improved by optimizing incubation conditions and by using micro spotting techniques for consistent delivery of antibodies to microelectrodes in an array. The value of $C$ provides a good measure of the uniformity of the coverage of casein on the electrode surface, and the value of $Q$ provides a good indication of immobilization of antibodies which might be a useful quality control tool. Thus, $C$, $Q$, $R$, $R_{ct}$ form an important set of circuit parameters that could be effectively used to engineer reliable bio functionalized surfaces.

### 3.3. *E. coli K12* detection

The Nyquist and Bode plots after *E. coli K12* bacteria capture (step 6) are shown in Fig. 2b–d. The same equivalent circuit (Fig. 2a) that was used at step 5 is again fitted to the experimental data of step 6 and the value of different parameters for microelectrodes # 3, 4, 5, 8 and 9 are shown in Table 2. The data from others #1, 2, 6 and 7 are not included for this study because the spectra were too noisy. Further understanding of different steps in the surface functionalization protocol, which could improve reproducibility, is underway in our lab. The effective electrode area is further reduced after bacteria capture due to its large physical size (1–4 μm long and 0.5–1 μm wide), which blocks some of the electron transfer paths between $Fe(CN)_6^{3-/4-}$ redox couple and electrode (Fig. S2b, in Supporting information) causing a further increase in the value of $R_{ct}$. Optical microscopy characterization showed 50–100 bacteria captured on a 200 μm electrode and ~5–10 bacteria on 10 μm electrodes (data not shown). Ideally, by using ≤10 μm microelectrodes, one bacterium could be captured from very dilute samples but this requires active pre-concentration steps such as di-electrophoretic traps (Voldman, 2006). The value of $R_{ct}$ for microelectrode 3 drastically increased, which is expected because there are more antibodies on the electrode surface compared to that of microelectrodes 4 and 9. At step 5, the value of $R_{ct}$ for microelectrode 3 was 57 MΩ and that of microelectrode 4 was 17.7 MΩ, *i.e.* microelectrode 3 has three times more $R_{ct}$ than microelectrode 4, and the surface of microelectrode 3 is covered with three times more antibodies than microelectrode 4, assuming negligible non-specific binding. Interestingly, after bacteria capture, the value of $R_{ct}$ increases proportionately, and the value of

$R_{ct}$ for microelectrode 3 still remains three times more than that of microelectrode 4. This demonstrates the high specificity of *E. coli K12* attachment and that the change in impedance due to non-specific binding is negligible. The $R_{ct2}/R_{ct1}$ ratio gives the value of the change in faradic impedance after bacteria capture, where $R_{ct1}$ and $R_{ct2}$ are the charge transfer resistances after antibody/casein and bacteria capture, respectively. This ratio must be a constant for all microelectrodes as long as there is no non-specific binding. Microelectrodes 3, 4 and 8 show almost the same average value of 4.0, and this satisfies the Langmuir adsorption isotherm (Rogers, 2000). According to this theory, the ratio of antibodies to antigen concentration is a constant and increasing the antibodies concentration leaves this ratio unchanged. Thus a constant value of 4.0 in spite of different amount of immobilized antibodies on MEA implies that Langmuir adsorption isotherm is satisfied. Further studies of Langmuir adsorption isotherm with various antibody concentrations are under investigation. The low ratio of 1.4 as shown by microelectrode 5 and also by another chip that had no bacteria capture suggest that this low value can be attributed to no significant bacteria capture. Further, microelectrode 9 showed a huge increase in $R_{ct}$ value (103 MΩ) and the ratio of $R_{ct}$'s is 6.09. Given that the value of $R_{ct}$ for this microelectrode after step 5 is 16.9 MΩ and is almost identical to that of microelectrode 4, the increase in $R_{ct}$ after bacteria capture should have been same as that of microelectrode 4. In fact, it is much bigger, *i.e.* 6.09 instead of 4.0. Also, the value of $R_s$ has increased tremendously, whereas $R$ has not increased significantly. The value of $R$ after bacteria capture has increased on an average by 30 times for all MEA except for microelectrodes 9 and 5. These unexpected values of the parameters indicate that this huge increase in $R_{ct}$ can be attributed to non-specific binding. In addition, the lowering of $Q$ after bacteria capture for all MEA except for microelectrodes 9 and 5 which remained the same further confirms this inference. The bacteria capture must increase $R$ by blocking the electrolyte solution in the pore, increases $R_{ct}$ and decreases $Q$ by reducing the effective area. The exact cause for this non-specific binding is not clear, but we suspect it may be due to certain chemical reactions not taking place under right thermodynamic conditions. It is interesting to note that except for microelectrode 9 the value of $R_s$ has remained almost constant throughout the entire surface modification process. Thus, this parameter is independent of the changes occurring at the electrode surface during bio-functionalization. We therefore propose that MEA can be used to determine average limiting values of all these parameters for different concentrations of antigens by performing repetitive experiments in the laboratory. Once these limiting values are determined, they can be used to distinguish between a real detection signal and that due to non-specific binding or any other unexpected events or errors during the bio-functionalization process. Therefore, the need for control experiments is significantly reduced. It is important to note that it is due to the unique properties of the UNCD interface such as its chemical stability, ultra-smooth surface morphology that helps to deposit a more uniform, dense and conformal coverage of monolayers and casein and minimum non-specific binding that a constant value of these parameters are observed, which is unlikely to be seen in other electrode materials. By adopting MEAs in the place of un-patterned macro electrode, a four orders of magnitude increase in sensitivity was observed. The largest increase in $R_{ct}$ (per unit cfu/ml) after bacteria capture was $17\,\Omega \pm 10\%$ for microelectrodes, as compared to $0.03\,\Omega \pm 10\%$ and $0.005\,\Omega \pm 20\%$ for shorted array and continuous film, respectively (Fig. S4, in Supporting information). This translates into 17 KΩ change at 1000 cfu/ml, which is comparable to the detection limits of most immunoassays. Further improvements in detection limits ($\leq$10 cfu/ml) could be achieved by decreasing the microelectrode size to 10 μm or less; optimizing the surface functionalization scheme and incorporating active pre-concentration steps.

## 4. Conclusions

We provide an electrochemical model that presents the relationship for exchange current, overpotential and charge transfer resistance for bio functionalized diamond microelectrodes, which could lead to better understanding of the impedance detection mechanism. We propose a new scheme based on circuit elements that reduce the need for control experiments by differentiating between a positive signal and a false-positive signal without performing an experiment. We demonstrate improvements in signal reproducibility, selectivity and sensitivity by using a highly stable ultrananocrystalline diamond microelectrode array. As a result, our UNCD MEA-EIS platform advances the commercialization of label-free electrochemical biosensors. The proof-of-principle demonstration of *E. coli K12* detection will be easy to integrate into a compact, self-contained system that is simple, portable and versatile. Besides, the ability to scale up to 100s of microelectrodes in highly multiplexed format on silicon substrates should reduce cost and render this system capable of analyzing complex samples.

## Acknowledgments

The authors would like to thank I. Wylie for critical reading of the manuscript. The work was supported by the Defense Threat Reduction Agency (DTRA) under contract HDTRA1–09-C-0007. This work was performed in part at the Center for Nanoscale Materials (CNM), Argonne National Laboratory, IL, USA. The use of the CNM was supported by the U.S. Department of Energy, Office of Science, Office of Basic Energy Sciences, under Contract No. DE-AC02-06CH11357.

## Appendix A. Supplementary data

Supplementary data associated with this article can be found, in the online version, at doi:10.1016/j.bios.2012.03.001.

## References

Alehashem, S., Chambers, F., Strojek, J.W., Swain, G.M., 1995. Anal. Chem. 67, 2812–2821.
Barsoukov, E., MacDonald, J.R., 2005. Impedance Spectroscopy: Theory, Experiment, and Applications. Wiley-Interscience.
Clare, T.L., Clare, B.H., Nichols, B.M., Abbott, N.L., Hamers, R.J., 2005. Langmuir 21 (14), 6344–6355.
Cui, Y., Wei, Q., Park, H., Lieber, C.M., 2001. Science 293, 1289–1292.
Daniels, J.S., Pourmand, N., 2007. Electroanalysis 19, 1239–1257.
Ghindilis, A.L., 2009. Electroanalysis 21 (13), 1459–1468.
Granger, M.C., et al., 2000. Anal. Chem. 72 (16), 3793–3804.
Gruen, D.M., et al., 1996. Appl. Phys. Lett. 68 (12), 1640–1642.
Juttner and Becker, J., 2007. J. Appl. Electrochem. 37 (1), 27–32.
Hernando, J., Lud, S.Q., Bruno, P., Gruen, D.M., Stutzmann, M., Garrido, J.A., 2009. Electrochim. Acta 54, 1909–1910.
Holt, K.B., Bard, A.J., Show, Y., Swain, G.M., 2004. J. Phys. Chem. B 108 (39), 15117–15127.
Katz, E., Willner, I., 2003. Electroanalysis 15 (11), 913–947.
Kondo, T., Honda, K., Tryk, D.A., Fujishima, A., 2003. Electrochim. Acta 48, 2739–2748.
Li, J., Koehne, J., Cassell, A.M., Chen, H., Ye, Q., Ng, H.T., Han, J., Fan, W., Meyyappan, M., 2005. Electroanalysis 17, 15–27.
Long, Y.T., Li, Z.-C., Kraatz, H.-B., Lee, J.S., 2003. Biophys. J. 84 (5), 3218–3225.
Ma, K.S., Zhou, H., Zoval, J., Madou, M., 2006. Sens. Actuators B 114, 58–64.
Moldovan, N., Divan, R., Zeng, H., Carlisle, J.A., 2009. J. Vac. Sci. Technol. B 27 (6), 3125–3131.
Nebel, C.E., Rezek, B., Shin, D., Uetsuka, H., Yang, N., 2007. J. Phys. D: Appl. Phys. 40, 6443–6466.
Nirschl, M., Reuter, F., Vörös, J., 2011. Biosensors 1, 70–92.
Radadia, A.D., et al., 2011. Adv. Funct. Mater. 21, 1040–1050.
Ramesham, R., Rose, M.F., 1997. Diamond Related Mater. 6 (1), 17–26.
Rogers, K.R., 2000. Mol. Biotechnol. 14, 109–129.
Schulz, M.J., et al., 2007. Sens. Actuators B 123., 177–182.
Show, Y., Witek, M.A., Sonthalia, P., Swain, G.M., 2003. Chem. Mater. 15, 879–888.
Siddiqui, S., Arumugam, P.U., Chen, H., Li, J., Meyyappan, M., 2010. ACS Nano 4 (2), 955–961.

Stavis, C., et al., 2011. PNAS 108 (3), 983–988.
Stern, E., et al., 2010. Nat. Nanotechnol. 5, 138–142.
Sun, B., et al., 2007. Diamond Related Mater. 16, 1608–1615.
Szpak, S., 1991. Techniques for Characterization of Electrodes and Electrochemical Processes. Selman, Wiley & Sons.
Voldman, J., 2006. Annu. Rev. Biomed. Eng. 8, 425.
Yang, N., et al., 2011. Phys. Status Solidi A, 1–6.
Yang, W., et al., 2002. Nat. Mater. 1, 253–257.
Yu, X., et al., 2006. Analyst 131, 745–749.
Zheng, G., Patolsky, F., Cui, Y., Wang, W.U., Lieber, C.M., 2005. Nat. Biotechnol. 23, 1294–1301.